Iron oxidation under the influence of phosphate thin films

Jean-Luc Grosseau-Poussard, Benoît Panicaud, F. Pedraza, P. O. Renault, Jean-François Silvain

Iron oxidation under the influence of phosphate thin films

J. L. Grosseau-Poussard,[a] B. Panicaud, and F. Pedraza
Laboratoire d'Etudes des Matériaux en Milieux Agressifs, Pôle Sciences et Technologie, Université de La Rochelle, 17042 La Rochelle Cedex 1, France

P. O. Renault
Laboratoire de Métallurgie Physique, Associé au CNRS, Université de Poitiers, SP2MI, F-86960 Futuroscope Cedex, France

J. F. Silvain
ICMCB-CNRS, Université de Bordeaux 1, Av. Dr. A. Schweitzer 33608 Pessac, France

(Received 14 January 2003; accepted 11 April 2003)

Iron phosphate thin films have been obtained under controlled conditions by chemical conversion deposition. The films were formed on polycrystalline α-iron by immersion in acetone, as an organic solvent. After deposition, the films were investigated by x-ray photoelectron spectroscopy (XPS) and their influence on the thermal oxidation of α-iron was studied by means of *in situ* low incidence x-ray diffraction of synchrotron radiation. The study reveals interesting features related to the structure of both the phosphate and thermal oxide films. The XPS data suggest the iron phosphate to be constituted of long chains of phosphate groups PO_4^{3-}; these groups being interconnected by Fe^{2+} and Fe^{3+} cations. X-ray diffraction measurements have shown a significant modification of the oxidation behavior of α-iron at 400 °C and atmospheric pressure, which is derived from the presence of the thin film: α-Fe_2O_3 formation is clearly enhanced to the detriment of Fe_3O_4, compared to the oxidation of pure iron in which Fe_3O_4 is the dominant phase. As the growth rate of the α-Fe_2O_3 layer is significantly reduced compared to that of Fe_3O_4, thus the phosphated layers may find niche applications in low-to-moderate temperature environments. © *2003 American Institute of Physics.* [DOI: 10.1063/1.1579126]

I. INTRODUCTION

In order to shield a metallic surface, an adherent and insulating film must be applied. Research on conversion layers has received a lot of attention in the last decades. Among all conversion treatments, phosphate compounds have been the subject of various in-depth studies owing to their particular characteristics. These include practical applications[1,2] such as electrical insulators and lubricators, decreasing friction, wear, and cold deformation of metals as well as academic nature.[3,4] However, most of the literature is concerned with zinc or manganese phosphate coatings and very limited literature is available on iron phosphate.[5,6] The current lack of information severely hinders the development of new products and the effective application of existing products to new uses. The phosphating process involves dissolution of a base metal in an acidic solution of soluble primary phosphates, with the subsequent hydrolysis of these phosphates and the precipitation of insoluble tertiary phosphates coatings. However, it is by no means certain whether these phosphated materials are suitable for high temperature applications because few studies have been concerned with the high temperature resistance of phosphated materials.[7,8] In particular, from an academic point of view, it is not known how such a phosphate layer will affect the iron oxidation mechanism.

In this article, we report on a comprehensive study of iron phosphated thin films prepared following chemical routes, and its influence on iron oxidation. After elaboration, the films were investigated by x-ray photoelectron spectroscopy (XPS). Then, oxidation of such phosphated iron was performed at 400 °C under atmospheric pressure of artificial air. The growth of the oxide layers has been followed *in situ* by low incidence x-ray diffraction (XRD) of synchrotron radiation.

Typically, an aqueous solution is employed in the phosphating process. However, it has been recently found that such a treatment performed in acetone as an organic solvent, gives rise to a thin amorphous film of about 400 nm, which in turn, significantly increases the oxidation resistance of iron powders in the temperature range 300–700 °C.[9] However, a thorough understanding of the mechanisms responsible for the improvement of the oxidation resistance is still lacking. Knowledge about the similarities and differences between oxidation of pure iron and of phosphated iron, in particular with respect to the evolutions occurring in the oxide layer, may lead to a better understanding of the improvement of the oxidation properties by development of an oxide layer.

II. EXPERIMENTAL PROCEDURE

The phosphated specimens were prepared from 1 mm thick sheets of polycrystalline α-Fe (supplied by Goodfellow), with a chemical purity of 99.5%. Details on the phosphating process are given in Ref. 9.

[a]Author to whom correspondence should be addressed; electronic mail: jlgrouss@univ-lr.fr

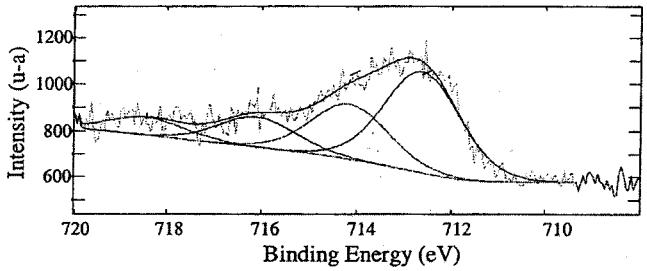

FIG. 1. XPS analysis from phosphated α-iron indicating the chemical species composing the Fe $2p$ core level.

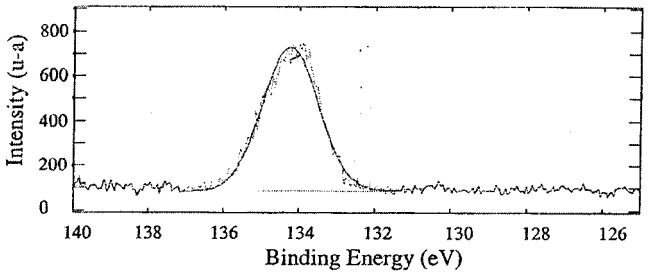

FIG. 2. XPS analysis from phosphated α-iron indicating the chemical species composing the P $2p$ core level.

Specimens used for XPS analysis were stored in a dessicator under dried nitrogen until being transferred into the UHV apparatus for surface analysis and immediately analyzed. XPS measurements were undertaken using a VG ESCALAB 220 i-XL instrument, using a monochromated Al $K\alpha$ radiation source (150 μm spot) without coaxial charge compensation. Data were acquired for the Fe $2p$ (700–740 eV), P $2p$ (124–140 eV), O $1s$ (528–540 eV), and C $1s$ (276–294 eV) regions. Deconvolution of the spectra was performed by fitting the data with a Gaussian/Lorentzian combination peak shape with variation in peak full width at half maximum (FWHM), position and height being determined by an iterative program. The peak identification was determined by reference to an XPS data base[10] or from calibrated standards analyzed in the same apparatus. In all cases, the spectra were charge referenced to a hydrocarbon contamination C $1s$ peak at a binding energy (BE) of 284.5 eV and no sputter cleaning was applied. Indeed, a transfer from higher to lower binding energy in the intensity in the Fe $2p$ peak as a function of sputtering has already been observed, corresponding to partial reduction of iron oxides.[11,12] For example, McIntyre[11] considers that bombardment of an Fe_2O_3 surface results in almost complete reduction to FeO. Sputtering of the surface is thus avoided in our study for the sake of accuracy.

The *in situ* oxidation tests were performed at the French synchrotron radiation facility, L.U.R.E. (Orsay, France) on the H10 beam line providing high x-ray beam intensity and quality, as well as the large wavelength range accessibility. In particular, it allows one to obtain diffraction peaks for extremely thin oxide layers and thus it provides information of the first oxidation stages. The high temperature x-ray diffraction (XRD) equipment used in this study consists of a high temperature chamber with an Ω-setting goniometer equipped with a position sensitive detector. The wavelength has been fixed at 0.190 335 nm. It was also verified by rocking curves that the growth oxide layers were not textured. In order to improve the XRD signal, all measurements were performed under a fixed low incidence of 3°. It is worth noting that whatever the oxidation time, the whole thickness of the oxide layers was checked because α-Fe lines from the substrate were always visible in the scans.

III. EXPERIMENTAL RESULTS

A. Chemical bonding in the phosphate films

Figures 1–3 show the XPS spectra and Table I reports the deduced parameters for phosphated α-iron. The Fe $2p$ spectrum can be fitted with four peaks (Fig. 1). The respective binding energies fall at about 712.62 and 714.15 eV with their respective satellites contributions at 716.09 and 718.43 eV providing contributions of 63.27% Fe^{2+} and 36.73% Fe^{3+} in iron phosphate. These results are in agreement with those of Brow *et al.*,[13] in which the Fe $2p$ binding energies obtained for different iron phosphate glasses were also decomposed into two separate components of the same energy range attributed to ferric and ferrous ions. These binding energies values are greater than those reported for most iron oxides but are in good agreement with those reported for oxidized iron phosphides. It also has to be noticed that no metallic component can be observed in the spectrum indicating its absence in the phosphate layer.

Only one component is present in the P $2p$ spectrum at 133.6 eV (Fig. 2), which is undoubtedly ascribed to iron phosphate as previously observed on a steel substrate treated with orthophosphoric acid[14] and on iron phosphate glasses.[13] This indicates that the conversion layer contains phosphate groups with a PO_4^{3-} structure.

It has been demonstrated[15] that the O $1s$ spectrum for both silicate and phosphate glasses can be used to distinguish between an oxygen ion with a formal charge (P–O), also called nonbridging oxygen (NBO), and those oxygen ions with no formal charge (P–O–P), which are known as the bridging oxygens (BOs). In the present study, this feature of the O $1s$ electrons was used to gain information about the nature of bonding in the conversion layer. In the oxygen region two components are necessary to fit the spectrum (Fig. 3). The first peak component is centered at 531.08 eV and the second is located around 532.57 eV with their respective contributions of 51.35% and 48.64%. These two contributions, respectively, reflect nonbridging (P–O) and bridging (P–O–P) oxygen contribution. Indeed, the binding

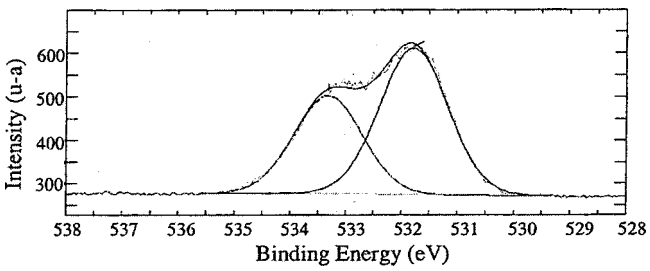

FIG. 3. XPS analysis from phosphated α-iron indicating the chemical species composing the O $1s$ core level.

TABLE I. Characteristic parameters of the Fe $2p$, P $2p$, and O $1s$ peaks deduced from the fitting procedure.

	Fe $2p$	Fe $2p$ satellite	Fe species	P $2p$	P species	O $1s$	O species
Phosphated α-iron							
Energy (eV)	712.62	716.09	Iron phosphate Fe^{2+}	133.6	Iron phosphated	531.08	Nonbridging oxygen in phosphate
Contribution (%)	63.27			100		51.35	
Energy (eV)	714.15	718.43	Iron phosphate Fe^{3+}			532.57	Bridging oxygen in phosphate
Contribution (%)	36.73					48.64	

energy of O $1s$ electrons in a –P–O–P– bond is higher than that in a –P═O– or –P–O–Fe– bond.[13–15] Moreover, the splitting between these two contributions is 1.8 eV, in agreement with previously published values for numerous phosphate glasses.[13–15] It also has to be noticed that no peak characteristic of oxide iron oxygen (Fe–O) is present around 530.0 eV which is, in turn, in agreement with the results providing from the Fe $2p$ region, confirming the absence of metallic iron oxide in the surface layer. It means that all iron cations are bound in the layer in phosphates and not as pure iron oxides. Thus the two contributions in the Fe $2p$ region cannot be considered independently of the phosphate groups and correspond to either $-Fe^{2+}-O-P$ or $-Fe^{3+}-O-P$ bonds.

From the above analysis it can be concluded that in the conversion layer formed on iron, some of the oxygen atoms (NBOs) are bonded via P–O–Fe links and the remaining (BOs) are bonded via P–O–P links. In these BOs, one oxygen is shared by the two tetraedra forming two phosphate PO_4^{3-} groups leading to a chain of phosphate groups, as in pyrophosphates or polyphosphates.[16] According to this structural model and as the proportion of BOs is significant, the iron phosphate structure may be constituted of long and numerous chains of phosphates groups which are connected with iron cations through $-Fe^{2+}-O-P$ or $Fe^{3+}-O-P$ bonds.

B. Structure of the oxide layers

The XRD patterns recorded on pure and phosphated iron samples oxidized at 400 °C for 20 and 80 min are presented in Fig. 4. It appears that both iron oxides magnetite (M; Fe_3O_4) and hematite (H; α-Fe_2O_3) are present in the different diffractograms. Pure iron shows rapid nucleation and growth of an oxide layer when exposed to air at 400 °C. On the other hand, the oxide layer grown on phosphated iron is thinner as the corresponding peaks exhibit weaker intensities for the same oxidation time. As a result, it seems that the iron phosphate films provide a better oxidation resistance compared to pure iron, consistent with previous studies of the oxidation kinetics in phosphated α-iron.[9] Careful examination of the spectra in Fig. 4 gives additional important information for 80 min of oxidation: in pure α-iron, the Fe_3O_4 (220) line is significantly higher than the α-Fe_2O_3 (104) line, whereas the inverse situation seems to occur in phosphated iron. It has to be outlined that this fact persists for oxidation exposures longer than 80 min. It also has to be noticed that the phosphate layer was not visible by x ray diffraction even in the low incidence mode.

From the *in situ* synchrotron diffraction study, a more detailed analysis of the spectra has been performed: taking into account the theoretical non-normalized intensity for α-Fe_2O_3 and Fe_3O_4 and as the absorption coefficient and the density are about the same for both oxides ($\mu_{\alpha\text{-}Fe_2O_3} = 220\ cm^2/g$ and $\mu_{Fe_3O_4} = 228\ cm^2/g$, $\rho_{\alpha\text{-}Fe_2O_3} = 5.24\ g/cm^3$ and $\rho_{Fe_3O_4} = 5.18\ g/cm^3$), the α-Fe_2O_3/Fe_3O_4 ratio can be deduced by means of the following relation:

$$\frac{\%_{\alpha\text{-}Fe_2O_3}}{\%_{Fe_3O_4}} \approx \frac{E_{\alpha\text{-}Fe_2O_3}}{E_{Fe_3O_4}} \frac{I_{Fe_3O_4}}{I_{\alpha\text{-}Fe_2O_3}} \frac{f_{Fe_3O_4}}{f_{\alpha\text{-}Fe_2O_3}}, \tag{1}$$

where $E_{\alpha\text{-}Fe_2O_3}$ and $E_{Fe_3O_4}$ are the integrated intensity, and $I_{\alpha\text{-}Fe_2O_3}$ and $I_{Fe_3O_4}$ the theoretical non-normalized intensity, for, respectively, the hematite and the magnetite diffraction lines. $f_{\alpha\text{-}Fe_2O_3}$ and $f_{Fe_3O_4}$ are defined as

$$f_{\alpha\text{-}Fe_2O_3} = \frac{\sin(2\theta_{\alpha\text{-}Fe_2O_3} - \omega)}{\sin\omega + \sin(2\theta_{\alpha\text{-}Fe_2O_3} - \omega)},$$
$$f_{Fe_3O_4} = \frac{\sin(2\theta_{Fe_3O_4} - \omega)}{\sin\omega + \sin(2\theta_{Fe_3O_4} - \omega)}, \tag{2}$$

where $\theta_{\alpha\text{-}Fe_2O_3}$ and $\theta_{Fe_3O_4}$ are the positions for, respectively, the hematite and the magnetite lines, and ω is the low x-ray incidence. From the experimentally measured positions of

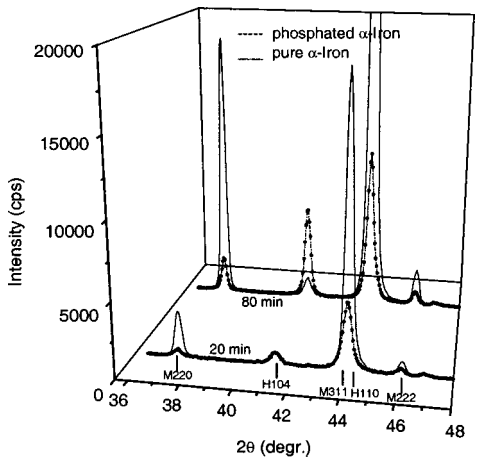

FIG. 4. Low incidence (3°) XRD patterns obtained after 20 and 80 min of *in situ* oxidation at 400 °C and atmospheric pressure for (—) pure α-iron, and (- - - -) phosphated α-iron. The 2θ and corresponding crystal orientation of the diffraction peaks are indicated. (N. B.: H refers to α-Fe_2O_3 and M to Fe_3O_4).

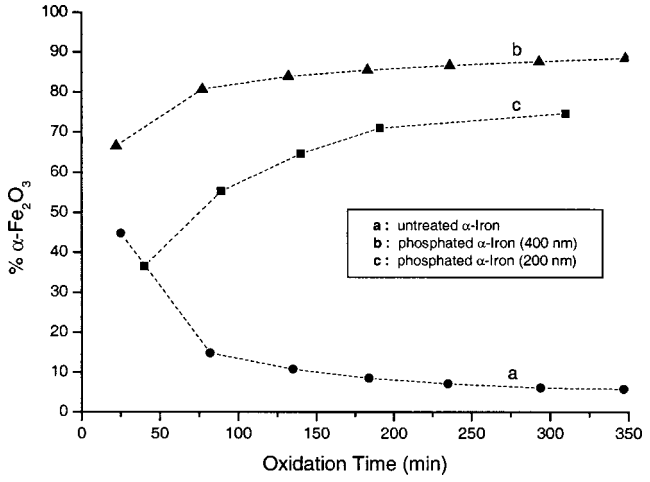

FIG. 5. Phases evolution percentage in the thermal oxide layer during oxidation at 400 °C at atmospheric pressure for (a) pure α-iron, (b) 400 nm thick iron phosphate film, and (c) 200 nm thick iron phosphate film. As α-Fe_2O_3 and Fe_3O_4 are the two main constituents of the oxide layer, the total percentage of phases is equal to unity.

the (220) and (222) Fe_3O_4, and (104) α-Fe_2O_3 peaks, and using the above relations we have determined average values of the evolution of the α-Fe_2O_3/Fe_3O_4 ratio during oxidation. It appears that for the pure specimen [Fig. 5(a)], Fe_3O_4 is the dominant phase whatever the oxidation time and its amount increases continuously with increasing oxidation time. On the other hand, for phosphated iron [Fig. 5(b)], α-Fe_2O_3 is the dominant phase from the beginning of oxidation to the end. Consequently, the phosphate layer induces an inversion of the phase ratio in the oxide layer. It is known that Fe_3O_4 supports a larger flux of rate controlling species and thus grows faster than α-Fe_2O_3.[17] Indeed, iron and oxygen self-diffusion coefficient in α-Fe_2O_3 are extremely low and the two self-diffusion coefficients are of the same magnitude ($D_{O/\alpha\text{-}Fe_2O_3}=3.34\times10^{-34}$ cm^2/s and $D_{Fe/\alpha\text{-}Fe_2O_3}=2.96\times10^{-34}$ cm^2/s), compared with the iron self-diffusion in magnetite ($D_{Fe/Fe_3O_4}=1.94\times10^{-22}$ cm^2/s).[17] Thus it seems reliable to obtain a decrease in kinetics and thus a thinner oxide layer on phosphated iron. So, in the present study the phosphate layer leads to the preferential growth of α-Fe_2O_3 during the oxidation process as is suggested by the present x-ray diffractogram.

To support this assumption, thinner iron phosphate films (<200 nm) were prepared and oxidized in the same conditions as above, giving rise to the phases evolution shown in Fig. 5(c). α-Fe_2O_3 is again the dominant phase but for a given oxidation time its ratio is lower than for the 400 nm phosphate film. Thus it clearly appears that the iron phosphate thin film is responsible for the enhanced growth of α-Fe_2O_3 in the oxide layer which modifies the iron oxidation mechanism.

According to the Fe–O phase diagram,[18] wustite (FeO) formation on pure α-Fe is only expected to occur at temperatures higher than 570 °C. Moreover, provided that the oxygen partial pressure in the oxidizing gas is sufficiently high to allow the formation of hematite (at 400 °C: $pO_2 \approx 10^{-18}$ Pa), the oxide layer is mainly constituted by a Fe_3O_4 sublayer between the substrate and a minor α-Fe_2O_3 outer layer in direct contact with the oxidizing atmosphere. It is known that growth of Fe_3O_4 first occurs at the metal/α-Fe_2O_3 interface because the partial pressure of oxygen decreases across the hematite oxide layer.

In the present work the development of Fe_3O_4 rapidly occurs in the oxide layer grown on pure iron (being the dominant phase after 20 min of oxidation). On the other hand for phosphated α-iron, α-Fe_2O_3 is the dominant phase during the whole oxidation process. A likely explanation can be described as follows: according to the XPS results, both Fe^{2+} and Fe^{3+} cations constitute the phosphate layer. Thus Fe_3O_4 and α-Fe_2O_3 are susceptible to occur. However, upon exposures at high temperatures, cracking of the chain may mainly occur across the nonbridging oxygen, providing an oxygen rich environment. Thus upon oxidation a higher pO_2 is found at the internal interface of phosphated samples and according to the redox reactions, much of Fe^{2+} should be oxidized to Fe^{3+}, giving rise to a higher ratio α-Fe_2O_3/Fe_3O_4 than in pure iron. Studies of Jutte *et al.*[19] using similar experimental conditions but with a layer of FeOOH have shown an increase in the oxygen partial pressure, giving rise also to a more enriched α-Fe_2O_3 scale.

IV. CONCLUSIONS

In summary, both XPS and *in situ* x-ray diffraction of synchrotron radiation have been employed to study the constitution of metallic iron phosphate films and its influence on the thermal oxidation of pure iron. It has been demonstrated that the oxidation resistance of α-iron can be increased by the use of a phosphating treatment in an organic solvent. The results have shown that the conversion layer may be formed of chains of phosphate groups; these chains being interconnected by divalent and trivalent iron cations. The oxidation mechanism of α-iron is sharply modified by the presence of such a phosphate film which promotes the slower formation of α-Fe_2O_3. Thus the thermal oxidation of iron is greatly reduced which could be very promising for the high temperature oxidation resistance of phosphated metallic pieces. Additional studies on the evolution of the phosphate layer during oxidation would be a plus to understand the influence of iron phosphate film parameters on the oxidation mechanisms of α-iron. Moreover the oxidation temperature range should be enlarged.

[1] G. Lorin, *Phosphating of Metals* (Finishing, Middlesex, 1974).
[2] T. Sugama, L. E. Kukocka, N. Carciello, and J. B. Warren, J. Mater. Sci. **23**, 101 (1988).
[3] A. Kolics, P. Waszczuk, L. Gancs, Z. Nemeth, and A. Wieckowski, Electrochem. Solid-State Lett. **3**, 369 (2000).
[4] K. Azumi, T. Ohtsuka, and N. Sato, J. Electrochem. Soc. **134**, 1352 (1987).
[5] S. Virtanen, P. Schmuki, M. Büchler, and H. S. Isaacs, J. Electrochem. Soc. **146**, 4087 (1999).
[6] C. A. Melendres, N. Camillone, and T. Tipton, Electrochim. Acta **34**, 281 (1989).
[7] M. R. Yang and S. K. Wu, Acta Mater. **50**, 691 (2002).
[8] W. B. Retallick, M. P. Brady, and D. L. Humphrey, Intermetallics **6**, 335 (1998).
[9] S. Rebeyrat, J. L. Grosseau-Poussard, J. F. Dinhut, and P. O. Renault, Thin Solid Films **379**, 139 (2000).
[10] J. F. Moulder, W. F. Stickle, P. E. Sobal, and K. D. Bomben, in *Handbook*

of X-Ray Photoelectron Spectroscopy, edited by J. Chastain and R. C. King, Jr. (1995).
[11] N. S. McIntyre and D. G. Zetaruk, Anal. Chem. **49**, 1521 (1977).
[12] C. R. Brundle, T. J. Chuang, and K. Wandelt, Surf. Sci. **68**, 459 (1977).
[13] R. K. Brow, C. M. Arens, X. Yu, and E. Day, Phys. Chem. Glasses **35**, 132 (1994).
[14] A. Stoch and J. Stoch, Solid State Ionics **34**, 17 (1989).
[15] M. Karabulut, G. K. Marasinghe, C. S. Ray, D. E. Day, O. Ozturk, and G. D. Waddill, J. Non-Cryst. Solids **249**, 106 (1999).
[16] R. K. Brow, D. R. Taillant, S. T. Myers, and C. C. Phifer, J. Non-Cryst. Solids **191**, 45 (1995).
[17] B. Amani, M. Addou, and C. Monty, Defect Diffus. Forum **194–199**, 1051 (2001).
[18] H. A. Wriedt, *Binary Alloy Phase Diagrams*, edited by T. B. Massalski (American Society for Metals, Materials Park, OH, 1990), Vol. 2, pp. 1739–1744.
[19] R. H. Jutte, B. J. Kooi, M. A. J. Somers, and E. J. Mittemeijer, Oxid. Met. **48**, 87 (1997).